ChemComm

Phenyleneethynylene trimer-based rigid-flexible [2+2] macrocycles for nucleic acid labelling in live cells

Journal:	*ChemComm*
Manuscript ID	CC-COM-03-2019-002162.R2
Article Type:	Communication

For Table of Contents use only

Facile synthesis of phenyleneethynylene (PE) trimer-based macrocycles for efficient nucleic acid labeling in live cells is presented.

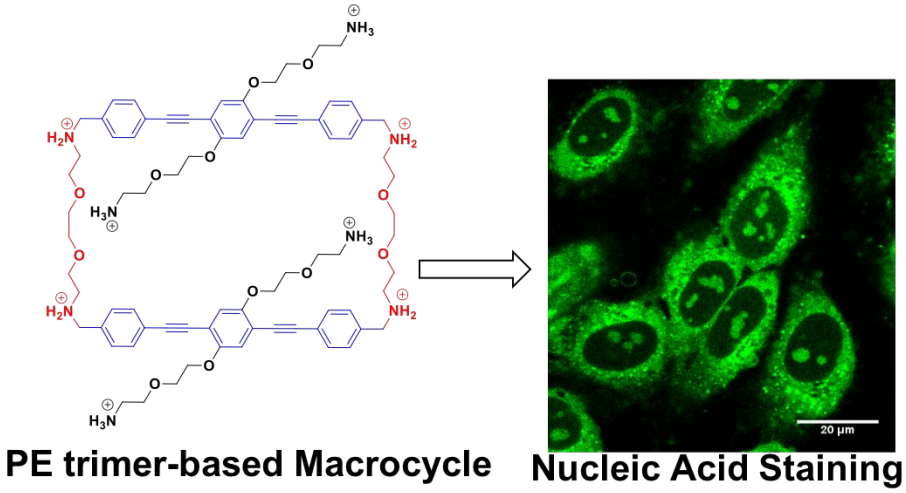

PE trimer-based Macrocycle **Nucleic Acid Staining**

COMMUNICATION

Phenyleneethynylene trimer-based rigid-flexible [2+2] macrocycles for nucleic acid labelling in live cells†

Received 00th January 20xx,
Accepted 00th January 20xx

DOI: 10.1039/x0xx00000x

Fluorescent macromolecules were developed for intracellular labeling in live cells. Coupling rigid rod phenyleneethynylene trimers with flexible amphiphilic diamines via the imine-bond formation chemistry yielded rigid-flexible [2+2] macromolecules showing nucleic acids selectivity and nontoxicity in live cells.

Fluorescent labelling of intracellular organelles, proteins, or nucleic acids (NAs) is an essential way of studying the structure and function of live cells.[1] As a new class of fluorescent materials, π-electron conjugated polymers (CPs) and conjugated polymer nanoparticles (CPNs) have recently gained much attentions for labelling, sensing, and delivery of biological substances owing to the excellent photophysical (i.e., high molar absorptivity, quantum yield, and photostability) and biophysical (i.e., nontoxicity and biocompatibility) properties.[2-6] However, relatively large molecular weights and broad molecular weight distributions of CP-based materials often limit their intracellular applications in live cells. To address the limitation associated with the size of CPs, our group previously introduced disulfide-containing CPNs exhibiting highly specific mitochondria labelling via efficient cellular entry followed by intracellular degradation to low molecular weight oligomers (i.e., pentamers).[7]

Nevertheless, molecularly defined short conjugated oligomers (COs) are better suited for intracellular labelling than CPs or CPNs.[8] For phenyleneethynylene (PE)-based oligomers, quantum yields (QYs) of short oligomers are generally higher than those of CPs because QYs decrease as the conjugation lengths increase due to the decreased contribution of vibrational deactivation.[9] COs with appropriate functional groups are highly water-soluble making applications in aqueous environments ideal. Low molecular weight amphiphilic COs likely enter cells by fast diffusion through the cell membranes, whereas CPs and CPNs are most likely endocytosed and entrapped in endosomes or lysosomes. Despite these advantages, COs have scarcely been used for fluorescent labelling applications in live cells.[10-12] The synthetic efficiency becomes poor as the conjugation length increases. COs should be modified with certain targeting or functional groups at the side chain or end of the conjugated backbone in order to achieve targeting or sensing functions.

Scheme 1. Synthetic scheme of macrocycles and PE trimer control.

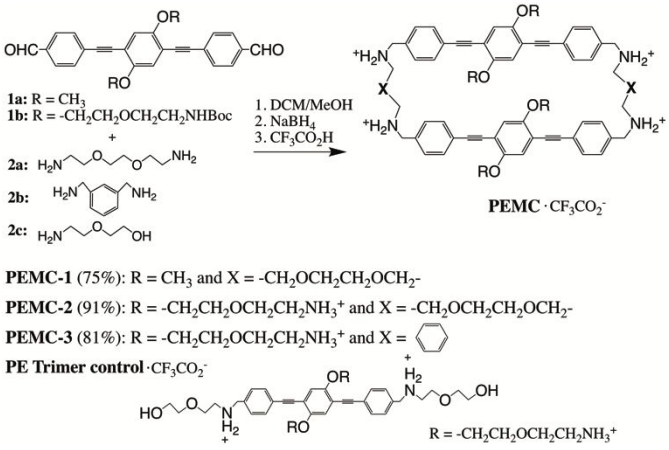

† Electronic Supplementary Information (ESI) available: Synthesis, characterization, cellular study, and theoretical simulations. See DOI: 10.1039/x0xx00000x

COMMUNICATION

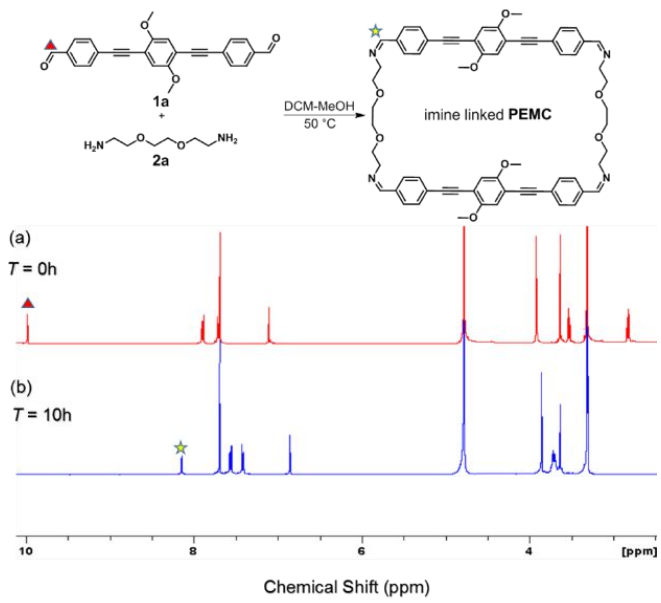

To combine the advantages of both CPs (i.e., more chromophores) and COs (defined molecular weights and faster cellular entry) avoiding extensive synthetic procedures, we designed a macrocyclic system using the imine-coupling chemistry between aldehyde end-capped PE trimer units and flexible diamines (Scheme 1). Because the equilibrium in the imine bond formation can be quantitatively shifted to thermodynamically favoured products, the target macrocycles can be obtained in high yields without accompanying by-products.[13] In this contribution, we report the synthesis of PE trimer-based rigid-flexible [2+2] macrocycles (PEMC) for nucleic acids labelling in live cells. The aldehyde-end-capped rigid PE trimers were coupled with flexible amphiphilic diamines, resulted in macrocycles in high yields. Primary amines at the end of side chains of the PE trimer play important roles in the nucleic acid staining. Macrocycles are approximately three times brighter than the corresponding trimer control and exhibit fast cellular entry, RNA selectivity, and nontoxicity, supporting that cyclization of COs can be a promising technique for improving intracellular targeted labelling.

Macrocycles were formed quantitatively via the imine-bond formation chemistry when the equimolar amounts of the aldehyde end-capped PE trimer (**1a** or **b**) was mixed with the diamine-containing linker (**2a** or **b**) in a mixed solvent of dichloromethane (DCM) and methanol (MeOH) (1:3, v:v) (Scheme 1). The progress and completion of the reaction was monitored by proton nuclear magnetic resonance (^{1}H NMR) showing the appearance of the imine proton peak at 8.15 ppm and corresponding chemical shifts of other proton peaks without forming by-products (Fig. 1). The effects of diamine for macrocyclization were evaluated using different diamines including **2b** and ethylenediamine. While aromatic **2b** formed corresponding macrocycle **PEMC-3** in high yields, short ethylenediamine failed to form a macrocycle, presumably due to the steric repulsion between the two PE trimers. A PE trimer control was also synthesized by reacting the PE trimer **1b** with 2-aminoethoxyethanol. Compared with the PE control, **PEMC-2**

Fig. 1. ^{1}H NMR spectra of reaction mixture at a) 0h and b) 10 h. The aldehyde proton of the PE trimer (filled triangle) was completely disappeared and a new proton peak from the imine bond (star marked) was appeared after 10 h reaction. No other proton signals were observed from the reaction mixture, indicating the quantitative transformation of macrocycles.

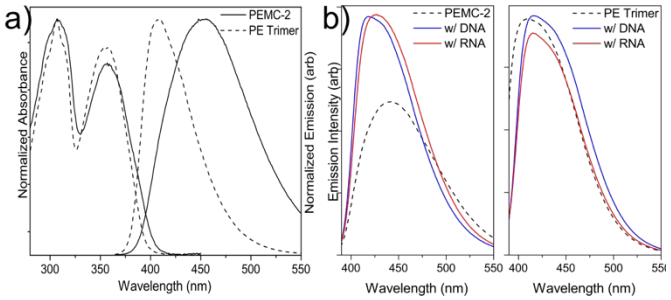

Fig. 2. Absorption and emission spectra of PEMC-2 and PE trimer in water (a) and emission spectra of PEMC-2 and PE trimer in the presence of NAs (b).

exhibits red shifted and broader emission profiles, indicating that the two PE trimers in the cycle form an excited state dimer (i.e., excimer) (Fig. 2a). The increased fluorescent intensity and blue shift of **PEMC-2** upon interacting NAs indicate that interaction between the two PE trimers in the cycle was weakened upon NA binding (Fig. 2b). The QY of **PEMC-2** was ~3-fold higher than the corresponding PE trimer, despite of having doubled the amounts of amine groups that generally lower QYs (Electronic Supporting Information, ESI, for characterization details).

Plate-shaped crystals of **PEMC-1** were obtained from acetonitrile and the solid-state structure was determined by single-crystal X-ray crystallography (see ESI). **PEMC-1** crystallizes in the P21/c space group, with one molecule in the unit cell. The crystal structure reveals the two PE units are not in close π-π stacking except for the centre phenyl group. The flexible side chains have an oppositely oriented geometry resembling the aza crown ether structure, resulting in distortion of the end phenyl groups in the trimer and the PE backbone. Although the geometry of PEMCs in an aqueous environment is not known, we speculate that **PEMC-2** in water may form a collapsed geometry similar to the crystal structure due to the hydrophobic PE trimeric units.

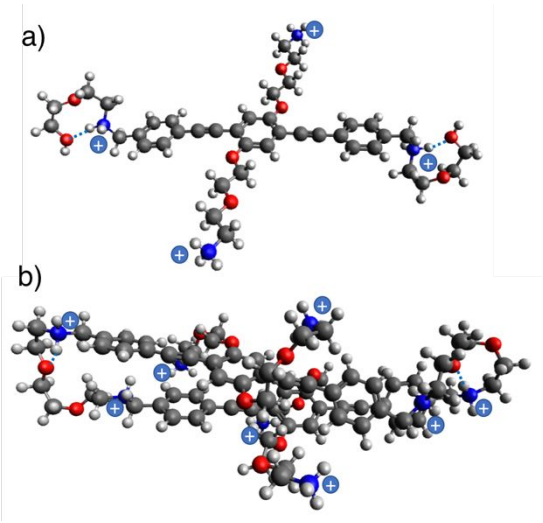

Fig. 3. Optimized molecular structure of the protonated PE-Trimer (total charge: +4) (a) and the protonated PEMC-2 (total charge: +8) (b) in aqueous solution. Hydrogen bonds are indicated by dotted blue lines. Red, blue, grey, and white spheres represent oxygen, nitrogen, carbon, and hydrogen atoms, respectively.

In order to gain an insight on the structure in an aqueous environment, quantum chemical calculations for geometry optimization and excitation energies of protonated PE control and **PEMC-2**, respectively, were conducted using the density-functional tight-binding (DFTB) method and molecular dynamics calculations.[14] In both PE-trimer and PEMC-2, the formation of intramolecular NH-O hydrogen bonding was observed in the linker moiety (Fig. 3). In the case of **PEMC-2**, we also noticed that a tendency for the sidechains to avoid unfavourable Coulombic repulsion of their positive charges by "wrapping" around the central PE-trimer moiety. Using these structures, we performed time-dependent DFTB calculations using the DFTB+ code and computed excitation energies and oscillator strengths for the 30 lowest singlet excited states (ESI). In the case of the PE-trimer, the HOMO-LUMO excitation occurs at 2.637 eV (= 470 nm), whereas the corresponding transition occurs in the **PEMC-2** macrocycle at 2.403 eV (= 516 nm). The redshift due to excimer formation is 46 nm, which is in good agreement with the experimental emission redshift (50 nm, Fig. 2a) due to a π–stacked structure (ESI).

Trifluoroacetate salted macrocycles are highly soluble in water and exhibit no noticeable cell viability inhibition (ESI). Using human cervical carcinoma cells (HeLa), the metabolic activity of HeLa cells in the presence of macrocycles was monitored, and no viability inhibition was observed up to 40 μM, which is considerably lower toxicity than many reported NA selective fluorescent molecules.[15-19] Cellular entry under the non-energy dependent conditions implies diffusion of macrocycles through the membranes. The entry efficiency of PEMCs and PE control determined by confocal microscopic images seems not to be decreased under both ATP depletion and 4 °C condition (ESI).

As shown in Fig. 4, **PEMC-2**, which contains the primary amine side chains, is localized in the nucleoli along with staining of the cytosol components. Meanwhile, **PEMC-1** without the amine side chain shows staining of only the cytosol, not in the nucleus, indicating the primary amine side chains play an important role in penetration of the nuclear membranes and

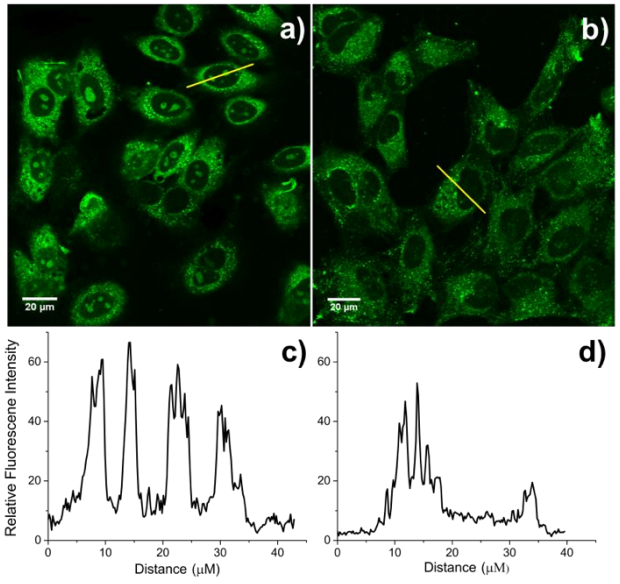

Fig. 4. Confocal microscopic images of HeLa cells incubated with **PEMC-2** (a) and **PEMC-1** (b). The fluorescent intensity profiles (c and d) along the yellow lines in the confocal images clearly indicate that **PEMC-2** localizes in the cytosol and nucleoli, while **PEMC-1** only localizes in the cytosolic compartments.

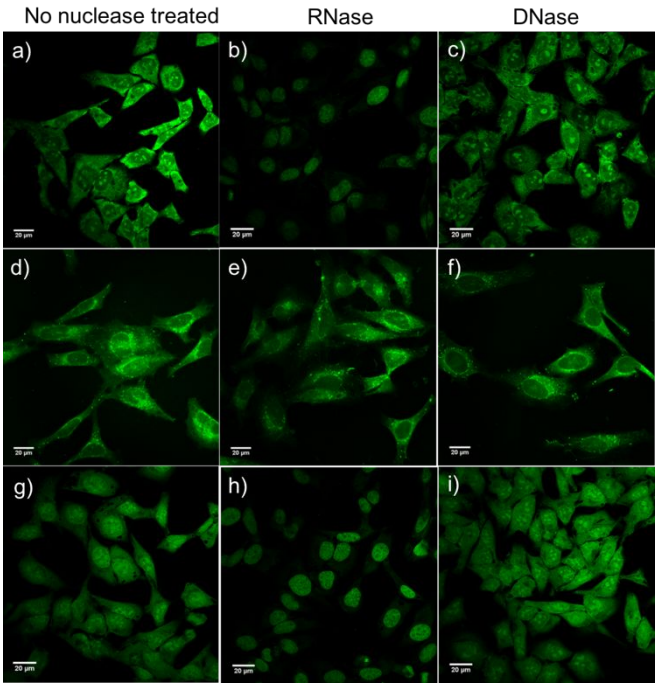

Fig. 5. Confocal microscopic images of Hela cells treated with **PEMC-2** (a-c), **PEMC-1** (d-f), and PE trimer control (g-i). After RNase treatment, **PEMC-2** are mainly seen in the nucleus (b) while no substantial changes are observed from the DNase treatment (c). The staining pattern of **PEMC-1** exhibits no effects upon the endonuclease treatment (e and f). PE trimer control exhibits relatively uniform staining of nucleus (g) and similar imaging patterns (h and i) to those of **PEMC-2** after the endonuclease treatment.

localization in the nucleoli. The relative fluorescent intensity profile along the yellow line in confocal images clearly indicates high localization of **PEMC-2** in the nucleoli (Fig. 4c) that are the site for ribosomal RNA transcription and processing.[20] Selective labelling of nucleoli is important for studying cellular functions and processes as the number, morphology, and size of nucleoli are tightly associated with the cell growth and metabolism.[21, 22] Because structurally similar DNA is abundant in the nucleus, the bright nucleoli spots found inside of the nucleus imply that **PEMC-2** has better selectivity to RNA over DNA. When competing double stranded DNA and other proteins co-exist, selective binding of small molecules to single stranded RNA is very challenging. It is known that the RNA selectivity is driven by the high electronegative potential surface of the major groove of RNA, which is rich in tandem GC base pairs offering multiple hydrogen bonding sites.[23] The flexible four amine side chains wrapped in the PE trimer units of **PEMC-2** could enhance binding to the RNA.

In order to examine the RNA selectivity, permeabilized HeLa cells incubated with the macrocycles were further treated with ribonuclease (RNase) and deoxyribonuclease (DNase), and confocal microscopic images were obtained. As shown in Fig. 5, **PEMC-2** clearly shows nucleus staining after digesting RNA (Fig. 5b), while a very similar imaging pattern was obtained after digesting DNA (Fig. 5c). The imaging patterns of **PEMC-1**, which has no primary amine side chains, present no difference before and after RNase and DNase digestion, indicating **PEMC-1** localizes in the intracellular compartments without involving NA

staining. In order to check whether **PEMC-2** exhibits higher fluorescence intensity upon interacting with RNA, the fluorescent intensity of the macrocycle was examined as the amounts of RNA increased (Fig. 2b). The fluorescent intensity of **PEMC-2** was slightly increased upon mixing with the excess amounts of NAs, but no intensity differences between RNA and DNA were observed from the macrocycle. The increased emission intensity, blue-shifted emission maximum, and decreased spectral width of **PEMC-2**/NA imply the slightly reduced π-π stacking between the two PE trimers in the cycle upon interacting with NAs. The PE trimer control exhibits very small changes in emission upon NA complexation (Fig. 2b). From the observations, we concluded that **PEMC-2** has higher affinity to RNA over DNA. The distinguishable nucleus staining after RNase treatment indicates that relatively small amounts of **PEMC-2** were also bound to DNA and the fluorescent signals became visible once the intense signals from RNA-bound **PEMC-2** were removed by digestion of RNA. The PE trimer control sharing the same primary amine-containing side chains exhibits a somewhat similar imaging pattern to that of **PEMC-2** (Fig. 5g-i). However, the overall fluorescent intensity and the contrast between nucleus and nucleolus is much lower, implying that cyclization of PE trimers to a macrocycle can enhance the brightness and RNA selectivity of COs.

In conclusion, we have demonstrated a highly efficient synthetic method of macrocycles by combining multiple fluorophores into a cyclic molecule with a defined molecular weight. We also discovered that the RNA selectivity in live cells could be improved by a straightforward cyclization of two rigid PE oligomers with the flexible amine side chains. Considering the availability of various COs with different colours and functional groups, our demonstration could lead to realization of highly selective labelling and sensing of target intracellular organelles in live cells, which will provide pivotal biological information of cells.

Conflicts of interest

There are no conflicts to declare.

Notes and references

1. H. Zhu, J. L. Fan, J. J. Du and X. J. Peng, *Acc. Chem. Res.*, 2016, **49**, 2115-2126.
2. K. Y. Pu and B. Liu, *Adv. Funct. Mater.*, 2011, **21**, 3408-3423.
3. C. L. Zhu, L. B. Liu, Q. Yang, F. T. Lv and S. Wang, *Chem. Rev.*, 2012, **112**, 4687-4735.
4. B. Wang, J. Han, M. Bender, S. Hahn, K. Seehafer and U. H. F. Bunz, *ACS Sensors*, 2018, **3**, 504-511.
5. J. H. Moon, W. McDaniel, P. MacLean and L. E. Hancock, *Angew. Chem.Int. Ed.*, 2007, **46**, 8223-8225.
6. J. H. Moon, E. Mendez, Y. Kim and A. Kaur, *Chem. Commun.*, 2011, **47**, 8370-8372.
7. M. Twomey, E. Mendez, R. K. Manian, S. Lee and J. H. Moon, *Chem. Commun.*, 2016, **52**, 4910-4913.
8. B. Wang, B. N. Queenan, S. Wang, K. P. R. Nilsson and G. C. Bazan, *Adv. Mater.*, 2019, e1806701.
9. M. Hergert, M. Bender, K. Seehafer and U. H. F. Bunz, *Chem. Eur. J.*, 2018, **24**, 3132-3135.
10. A. Barattucci, E. Deni, P. Bonaccorsi, M. G. Ceraolo, T. Papalia, A. Santoro, M. T. Sciortino and F. Puntoriero, *J. Org. Chem.*, 2014, **79**, 5113-5120.
11. C. Nie, S. Li, B. Wang, L. Liu, R. Hu, H. Chen, F. Lv, Z. Dai and S. Wang, *Adv. Mater.*, 2016, **28**, 3749-3754.
12. J. Wang, L. Zhou, H. Sun, F. Lv, L. Liu, Y. Ma and S. Wang, *Chem. Mater.*, 2018, **30**, 5544-5549.
13. S. J. Rowan, S. J. Cantrill, G. R. L. Cousins, J. K. M. Sanders and J. F. Stoddart, *Angew. Chem.Int. Ed.*, 2002, **41**, 898-952.
14. S. Grimme, S. Ehrlich and L. Goerigk, *J.Comput. Chem.*, 2011, **32**, 1456-1465.
15. H. Li, Y. Li, H. Zhang, G. Xu, Y. Zhang, X. Liu, H. Zhou, X. Yang, X. Zhang and Y. Tian, *Chem. Commun.*, 2017, **53**, 13245-13248.
16. R. Feng, L. Li, B. Li, J. Li, D. Peng, Y. Yu, Q. Mu, N. Zhao, X. Yu and Z. Wang, *RSC Adv.*, 2017, **7**, 16730-16736.
17. G. Niu, W. Liu, B. Zhou, H. Xiao, H. Zhang, J. Wu, J. Ge and P. Wang, *J. Org. Chem.*, 2016, **81**, 7393-7399.
18. L. Guo, M. S. Chan, D. Xu, D. Y. Tam, F. Bolze, P. K. Lo and M. S. Wong, *ACS Chem. Biol.,* 2015, **10**, 1171-1175.
19. Y.-J. Lu, Q. Deng, D.-P. Hu, Z.-Y. Wang, B.-H. Huang, Z.-Y. Du, Y.-X. Fang, W.-L. Wong, K. Zhang and C.-F. Chow, *Chem. Commun.*, 2015, **51**, 15241-15244.
20. J. S. Andersen, Y. W. Lam, A. K. L. Leung, S. E. Ong, C. E. Lyon, A. I. Lamond and M. Mann, *Nature*, 2005, **433**, 77-83.
21. M. Derenzini, D. Trere, A. Pession, M. Govoni, V. Sirri and P. Chieco, *J. Pathol.*, 2000, **191**, 181-186.
22. Q. Li, Y. Kim, J. Namm, A. Kulkarni, G. R. Rosania, Y.-H. Ahn and Y.-T. Chang, *Chem. Biol.*, 2006, **13**, 615-623.
23. B. Shirinfar, N. Ahmed, Y. S. Park, G.-S. Cho, I. S. Youn, J.-K. Han, H. G. Nam and K. S. Kim, *J. Am. Chem. Soc.*, 2013, **135**, 90-93.